AI-Enhanced Fault Diagnosis in Rolling Element Bearings: A Comprehensive Vibration Analysis Approach

Prasanta Kumar Samal
Department of Mechanical Engineering
The National Institute of Engineering
[NIE], Mysuru Karnataka
India

Sunil K.
Department of Mechanical Engineering
The National Institute of Engineering
[NIE], Mysuru Karnataka
India

Imran M Jamadar
Department of Mechanical Engineering
The National Institute of Engineering
[NIE], Mysuru Karnataka
India

Srinidhi R.
Department of Mechanical Engineering
JSS Science and Technology
University,Mysuru Karnataka
India

This research presents a comprehensive approach for bearing fault diagnosis using artificial intelligence (AI), particularly through the application of artificial neural networks (ANNs). By integrating these networks into vibration analysis, the approach aims to meet the critical need for prompt fault detection. The methodology comprises three key steps: vibration signal acquisition, feature extraction, and fault classification. Experiments were conducted to acquire vibration signals for the test bearings on a machinery fault simulator. Six time-domain features were extracted using MATLAB, creating a comprehensive dataset for training the ANN models with three algorithms: Levenberg-Marquardt backpropagation (LMBP), scaled conjugate gradient backpropagation (SCGBP), and Bayesian regularization backpropagation (BRBP). The BRBP algorithm achieved the highest correct classification rate (97.2%), followed by LMBP (90%) and SCGBP (83.6%). To evaluate their efficacy in bearing fault classification, these three networks were simulated, revealing that BRBP could predict all four classes of bearings with zero errors.

Keywords: *Artificial Intelligence,Artificial Neural Network, Fault Diagnosis, Fault Classification, Rolling Element Bearing, Vibration Signal Acquisition, Time-Domain Features.*

1. INTRODUCTION

Rolling element bearings (REBs) find extensive application in rotating machinery and are regarded as vital components. Their reliable operation holds utmost significance in diverse sectors, including nuclear power plants, chemical industries, aviation industries, and various process industries. Timely fault detection in rotating machinery can mitigate the potential for damage and, consequently, reduce the need for costly emergency repairs. During regular operations, both mechanical and electrical systems generate distinctive signals. Any alteration in a machine's operating conditions will result in deviations from this characteristic signal. Indeed, variations in the typical signal can serve as an indicator of an impending fault [1]. Machine Condition Monitoring (CM) is the process of continuously monitoring various parameters, which can offer some insights into the condition of the machine during its operation, including factors like vibration and temperature. Modern condition monitoring systems typically consist of data acquisition systems with sensors and are integrated with software for signal analysis.

Numerous researchers have reviewed bearing fault diagnosis using various monitoring techniques, including vibration and acoustic measurements[2-10]. Their review covered vibration measurements in both the frequency and time domains as well as acoustic measures involving sound pressure, sound intensity, and acoustic emission techniques; it also explored high-frequency resonance techniques.

Vibration is the most commonly used condition monitoring of rotary machines. This technique is extensively used in applications like material handling, aerospace, and power generation [11]. Comprehending the origins of vibration is crucial for grasping vibration patterns to enable effective fault detection. Even for healthy bearings, there will still be vibration, termed variable compliance, which is considered normal [7]. Different vibration analysis methods are available. Howard [8] uses accelerometers for analog signal acquisition. Saruhan et al. [12] use four defect states to diagnose faults in rolling element bearings.

The time-domain signal records energy history and is frequently used for extracting statistical insights. It can detect defects and assess their severity using indicators like root mean square (RMS), kurtosis (KU), crest factor (CF), impulse factor (IF), peak value, energy index (EI), K-factor, and shape factor, with KU and CF being more sensitive to larger defects [9-10, 13-14]. The frequency domain signals can be obtained by converting the time-domain vibration signals using the fast Fourier transformation[15].Calculating bearing characteristic frequenciesis helpful as they can indicate the fault's location. Bearing defects produce periodic vibration impulses that contain energy across a broad frequency range, exciting the resonant frequencies of individual elements, known as the fundamental vibra–tion frequencies. When the outer race remains fixed while the inner race rotates, four distinct defect frequ–encies become apparent: BPFO (ball pass frequency

Received: December 2023, Accepted: June 2024
Correspondence to: Prasanta Kumar Samal
Department of Mechanical Engineering, The National Institute of Engineering, Mysuru, Karnataka, India.
Email: prasantaku.samal@gmail.com
doi: 10.5937/fme2403450S

outer race), BPFI (ball pass frequency inner race), BSF (ball spin frequency), and FTF (fundamental train frequency) [16].

Acquiring the vibration signal, signal processing, and diagnosis of fault utilizing machine learning can be performed in the MATLAB environment. Seokgoo et al. [17] used MATLAB for diagnosing faults in REBs. AI techniques are employed for pattern recognition in machine diagnostics, with artificial neural networks being the prominently used techniques. Among these, the feed-forward neural network (FFNN), specially trained with the back-propagation (BP) algorithm, is extensively utilized for machine fault diagnosis [18-22].

The aforementioned literature provides a comprehensive background on the significance of the timely detection of faults in REBs and the utilization of vibration analysis to achieve this. As the demand for enhanced machinery reliability grows in today's AI-driven era, combining AI with vibration analysis greatly enhances REB fault diagnosis. Specifically, ANNs have found extensive applications in fault identification and classification. Unlike other ANN models that typically classify bearings as either faulty or healthy, the proposed ANN models classify various types of faulty bearings, such as faults in the inner race, outer race, or ball, and distinguish them from healthy ones. Furthermore, the performance of these three algorithms has been investigated, a topic rarely addressed in previous literature, thereby establishing the novelty of this research.

Hence, this paper endeavors to integrate AI techniques, particularly ANN, into fault diagnosis of rolling element bearings, presenting a comprehensive, data-driven methodology. The proposed approach combines vibration analysis with AI, including three main steps: acquisition of vibration signal, extraction of time-domain features, and classification of bearing faults. The subsequent quantitative evaluation highlights the practical applicability and effectiveness of this novel approach in the realm of industrial machinery health monitoring and predictive maintenance.

Section 2 provides a detailed methodology, including experimentation and data acquisition in sub-section 2.1, and outlines the procedure for extracting time-domain features and training the ANN models in sub-section 2.2. The results and discussion are presented in section 3, with conclusions summarized in section 4.

2. METHODOLOGY

The flow chart for the approach used in this research is shown in Figure 1. Using a machinery fault simulator, the vibration signals of the test bearings under various conditions - such as healthy bearings and faulty bearings with defects in the outer race, inner race, and rolling element - have been acquired. Section 2.1 details the experimental setup and data acquisition methods.

Subsequently, six key time-domain features – namely, RMS, kurtosis, crest factor, peak-to-peak, impulse factor, and energy - have been extracted from the acquired vibration data utilizing MATLAB. Section 2.2 provides a comprehensive explanation of this process.

An ANN model with a feedforward (FF) backpropagation (BP) algorithm has been developed to enhance predictive capabilities. For training, testing, and validation, the extracted dataset has been utilized. The details of this model development and dataset utilization are further explained in Section 2.2.

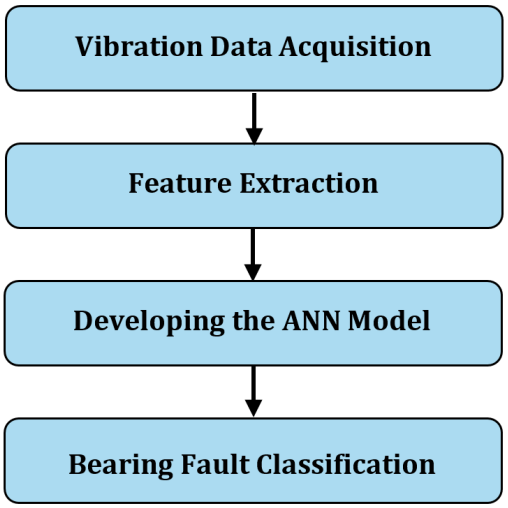

Figure 1. Methodology Flowchart

2.1 Experimentation and Data Acquisition

The machinery fault simulator (MFS) developed by Tyrannus Innovative Engineering & Research Academy PVT LTD, shown in Fig. 2, has been used for experimentation. It comprises a 3-phase 0.25 HP motor, two aluminum pedestals, a flexible coupling, two bearings, and a variable frequency drive (VFD). The flexible coupling connects the driven shaft with the motor output shaft, compensating for any potential misalignment. The two aluminum pedestals house the bearings, supporting the shaft. A functioning bearing is always positioned at the drive end (closer to the motor), while the test bearing is installed at the non-drive end. Motor speed is regulated by the VFD.A PCB Piezotronics tri-axial accelerometer is mounted onto the pedestal, as illustrated in Figure 2, to acquire the vibration of the test bearing. The accelerometer, through a lightweight cable, is connected to a dedicated data acquisition card, the NI9234, designed for sound and vibration acquisition. This card is mounted onto the NI cDAQ 9178 chassis. The chassis, in turn, is connected to a computer, with LabVIEW installed, via a USB cable.To acquire the analog acceleration signal in both the time domain as well as in the frequency domain and to save the data for further analysis, a LabVIEW application has been developed. The authors have utilized the same experimental setup for fan blade fault analysis [23].

In this investigation,the test bearing selected is the SKF 6304, a widely studied rolling element bearing that has been investigated using a different approach in previous literature [14]. The specifications of the test bearing are outlined in Table 1. Localized faults of circular shapes with a diameter of 0.5 mm have been artificially created by laser engraving on the balls, inner races, and outer races.The test bearings both with and without fault have been reinstalled separately in the setup to acquire vibration data.

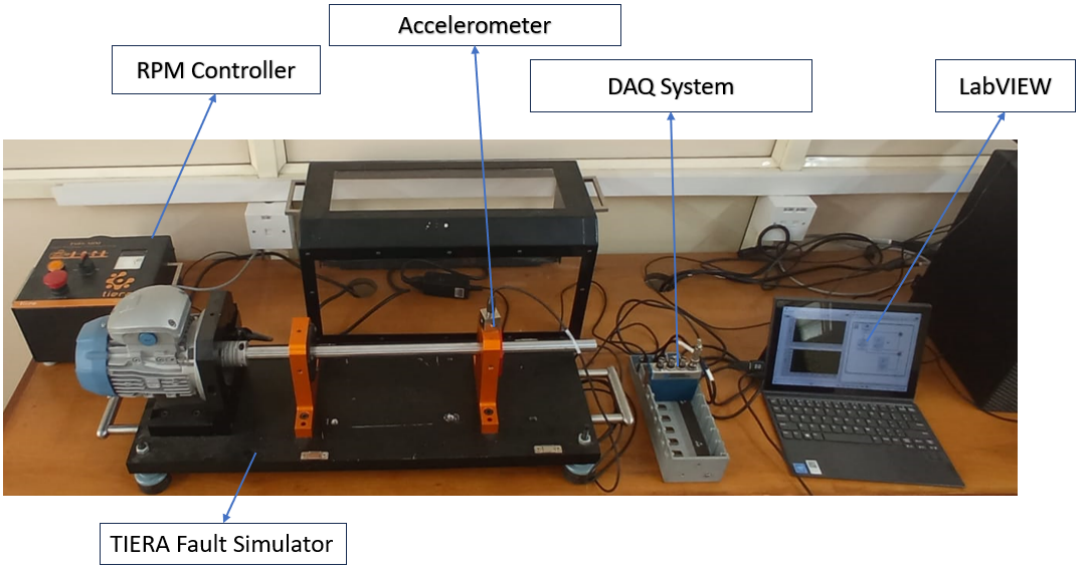

Figure 2. Experimental setup

Table 1. Specification of Test Bearing

Bearing number	6304
Type	deep groove
Inner diameter (ID)	20 mm
Outer diameter (OD)	52 mm
Race width (B)	15 mm
Ball diameter (d)	9.525 mm
Pitch diameter (D)	35.99 mm
No. balls (z)	7
Contact angle(ϕ)	0 degree
Material	chrome steel

2.2 Feature Extraction and ANN Model

The time domain technique stands out as the most straightforward and simplest approach for analyzing vibration signals. Many time domain features, including crest factor, kurtosis, peak-to-peak value, RMS, and others, can be utilized for condition monitoring [2]. The RMS measures the overall level of a discrete signal, which can be computed as the square root of the average of the values that are squared using (1),

$$RMS = \sqrt{\frac{1}{N}\sum_{i=1}^{N}|y_i|^2} \tag{1}$$

where "N" represents the number of discrete points, that is the signal from each sampled point. These RMS values are compared with established standards to evaluate the bearing's condition.

Kurtosis represents the fourth moment of a distri–bution normalized by the fourth power of the standard deviation. It offers a balanced measure that combines lower and higher moments to assess the shape and tail behavior of a dataset and can be computed using (2). It has been demonstrated that kurtosis is highly valuable in fault diagnosis,

$$\text{Kurtosis} = \frac{\sum_{i=1}^{N}(y_i - \bar{y})^4}{N * \sigma^4} \tag{2}$$

where the instantaneous magnitude (y_i), the mean($\bar{y}$), the sample length (N), and the standard deviation (σ).

The crest factor is defined as a ratio of peak value to RMS, as given in (3).

$$\text{CrestFactor} = \frac{\max_i |y_i|}{\sqrt{\frac{1}{N}\sum_{i=1}^{N}(y_i)^2}} \tag{3}$$

The impulse factor compares the peak height relative to the signal's mean level, calculated as the peak value divided by the mean of the absolute value as given in (4).

$$\text{ImpulseFactor} = \frac{\max_i |y_i|}{\frac{1}{N}\sum_{i=1}^{N}|y_i|} \tag{4}$$

Peak-to-peak value is calculated by finding the difference between the maximum and minimumvalues in the discrete signal data.Energy is computed as the mean of the squared values of the discrete signal data.

From the raw vibration signals acquired by follo–wing the procedure outlined in section 2.1, a MATLAB program has been employed to extract six essential time domain features: RMS, crest factor, kurtosis, impulse factor, peak-to-peak, and energy. These features serve as the input nodes for the neural networks, with four classes of bearings represented as output nodes.

For the development and simulation, the Neural Networks Toolbox in MATLAB has been utilized. Specifically, a Multi-Layer Feedforward Backpropa–gation (FFBP) ANN operating under supervised learning techniqueshas been employed. This is known for its efficacy in delivering highly precise results [24]. There are three built-in training algorithms namely Levenberg-Marquardtbackpropagation (LMBP), scaled conjugate gradient backpropagation (SCGBP), and Ba–yesian regularization backpropagation (BRBP), for trai–ning a network. Weight and bias values are updated by the LMBP algorithm in accordance with Levenberg-Mar

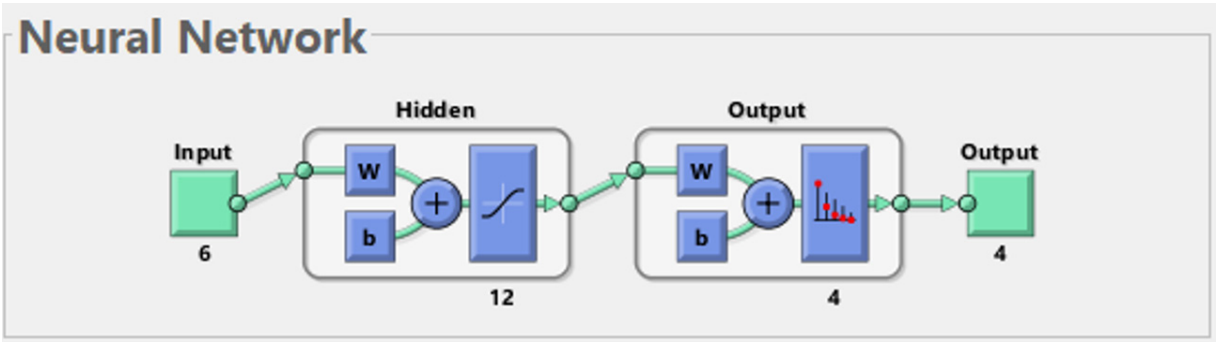

Figure 3. ANN Architecture

quardt optimization. Although it takeshigher me–mory than other algorithms, this is frequently the tool–box's quickest backpropagation method and comes hig–hly recommended as a first-choice supervised approach. The default algorithm is SCGBP, which uses the scaled conjugate gradient approach in updating the weight and bias values. BRBP uses Levenberg-Marquardt optimi–zation in updating the weight and bias variables. It determines the optimal blend to construct a network that exhibits strong generalization capabilities, initially by reducing a composite of squared errors and weights. Figure 3 illustrates the ANN architecture, while Table 2 provides details about the four target values corres–ponding to four classes of bearings.The four classes of bearings are healthy bearings (target value of 1000), bearing with an outer race defect (target value of 0100), an inner race defect (target value of 0010), and a ball defect (target value of 0001) as presented in Table 2.

Table 2. Target Values

Bearing Conditions	Target
Healthy Bearing	1000
Bearing with Defect on Outer race	0100
Bearing with Defect on Inner race	0010
Bearing with Defect on Ball	0001

3. RESULTS AND DISCUSSIONS

In the field of vibration analysis, the signals are ac–quired from machine components and both the time domain data and the frequency domain data are ana–lyzed. A fault in a bearing element is indicated by a peak observed in the vibration spectrum. However, the magnitude of this vibration peak depends on parameters like the size, shape, location, and type of defect. The theoretical bearing characteristic frequencies for the outer race defect, inner race defect, rolling element defect, and cage defectare typically labeled as BPFO, BPFI, BSF, andFTF, respectively. These theoretical bearing characteristic frequencies depend on both the bearing's geometry and the shaft speed, as given in equations (5-8) [25]. The theoretical bearing charac–teristic frequencies for the test bearing, with specified geometric details from Table 1 for a shaft speed of 1490 rpm, have been determined using the equations (5-8), and are presented in Table 3.

$$BPFO = \frac{z}{2} f_s \left(1 - \frac{d}{D}\cos\varphi\right) \tag{5}$$

$$BPFI = \frac{z}{2} f_s \left(1 + \frac{d}{D}\cos\varphi\right) \tag{6}$$

$$BSF = \frac{z}{2} f_s \left(1 - \frac{d^2}{D^2}\cos^2\varphi\right) \tag{7}$$

$$FTF = \frac{1}{2} f_s \left(1 - \frac{d}{D}\cos\varphi\right) \tag{8}$$

Table 3. Characteristic Frequencies of Test Bearing

Characteristic Frequencies (Hz)	
BPFO	64
BPFO	110
BSF	43,6
FTF	87.2

The experiments were conducted using the setup and procedure explained in Section 2.1. Bearings with various conditions, including both healthy ones and those with defects in different elements, were tested at a motor speed of 1490 rpm. Even for healthy bearings, some level of vibration, referred to as variable compli–ance [7], is observed. When a defect is present in the interface between the ball and the raceways, it results in a distinct peak in the amplitude of vibration due to the impact. These defects can occur in theinner race, in the outer race, or in the balls themselves. Figures 4-6 depict the time domain plots and frequency domain plots of vibration signals acquired from the outer race defect bearing, the inner racedefect bearing, andthe bearing with balldefect, respectively.

This can be observed from Figure 4(b) that the first prominent peak occurs at approximately 25 Hz, representing the shaft frequency. Additionally, there are peaks at approximately 65 Hz, 130 Hz, and 196 Hz, corresponding to the frequencies linked to a bearing having an outer race defect (fod) and its harmonics. The theoretical bearing characteristic frequency, ball pass frequency for an outer race defect (BPFO), is 64 Hz. This observation suggests an outer racedefect.In Figure 5(b), an initial prominent peak is seen at around 25 Hz, representing the shaft frequency. There are also noticeable peaks at 112 Hz and 225 Hz. These frequencies are related to an inner race defect (fid) and its harmonics. The expected theoretical bearing characteristic frequency for an inner race defect (BPFI) is 110 Hz, indicating the presence of adefect in the inner race.In Figure 6(b), the first significant peak is observed at around 25 Hz, representing the shaft frequency.

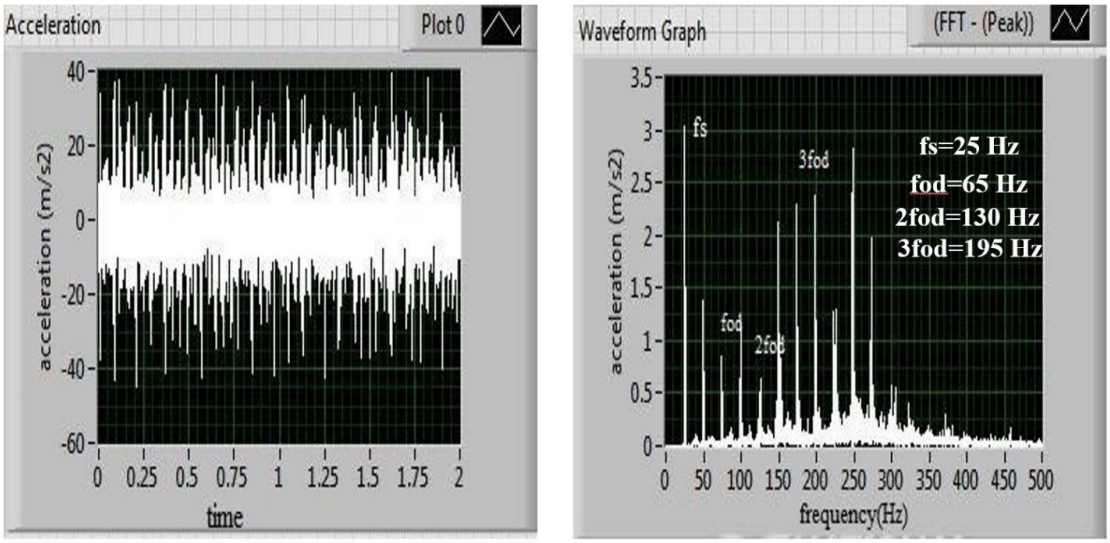

(a) (b)

Figure 4. Vibration Signal for Bearing with Outer Race Defect (a) Time Domain and (b) Frequency Domain

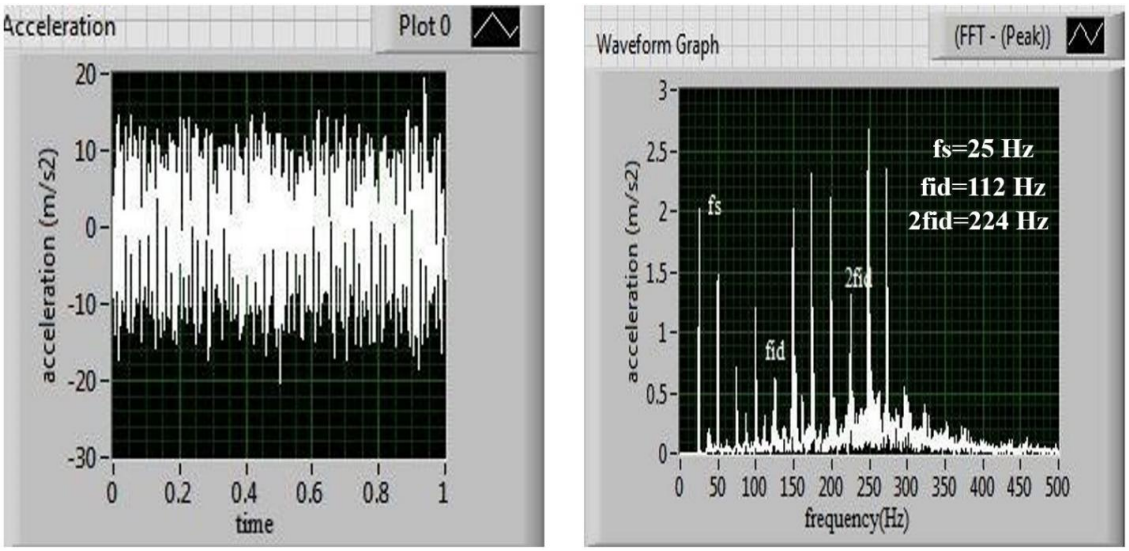

(a) (b)

Figure 5. Vibration Signal for Bearing with Inner Defect (a) Time Domain and (b) Frequency Domain

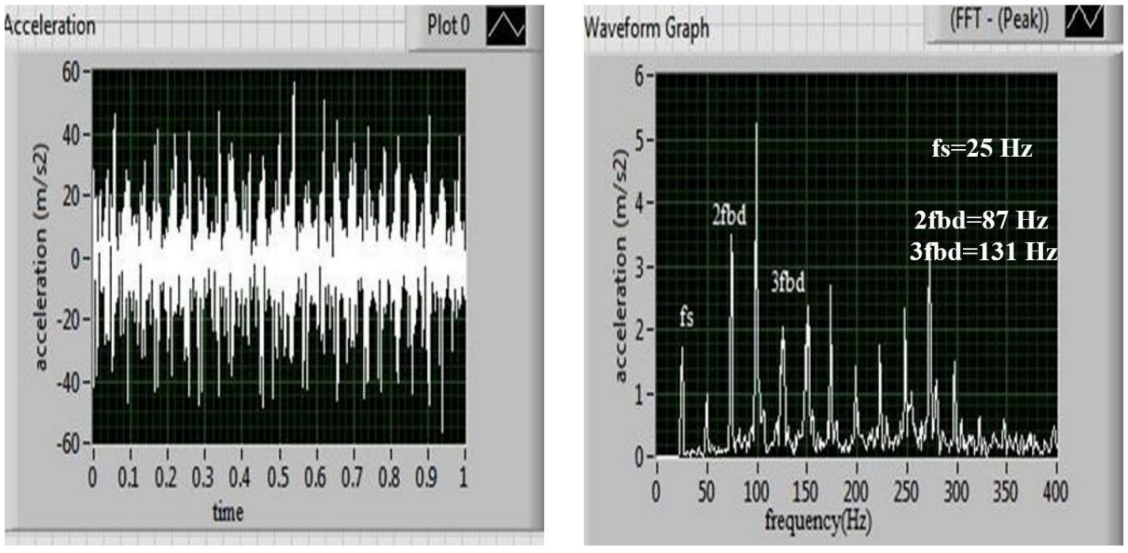

(a) (b)

Figure 6. Vibration Signal for Bearing with Ball Defect (a) Time Domain and (b) Frequency Domain

Additionally, there are peaks at approximately 87 Hz and 131 Hz.These are the harmonics of a ball defect frequency (fbd). The theoretical bearing characteristic frequency, ball spin frequency (BSF), is 87.2 Hz. This observation indicates a ball defect.

3.1 Fault Classification using ANN

The six essential time-domain features - RMS,crest fac–tor, kurtosis, impulse factor, peak-to-peak, and energy - have been extracted from the vibration signals using a MATLAB program. Table 4 presents the statistical parameters, namely range (minimum and maximum values), mean, and standard deviation, of the six time-domain features for four distinct bearing conditions.

The next step in ANN modeling is selecting the number of hidden neurons. A back-propagation neural network's predictionaccuracy is greatly influenced by the quantity of hidden layers. An inadequate number of nodes can hinder learning and lengthen the training process, which will impact accuracy. On the other hand, using too many layers can result in over-fitting and prolonged training times. The quantity of hidden layers can be calculated using the formula provided in equations (9,10) [26].

$$1 < \sqrt{(m+n)} + a \tag{9}$$

$$1 > \log_2 n \tag{10}$$

With the number of output nodes (m), the number of input nodes (n), 'a' being a constant, that varies from one to ten.In this case, the value of ‘m’ and ‘n’ are respectively four and six. These values have been substituted in equation (9) resulting in 'l' ranging from four to thirteen. However, as per equation (10), 'l' should be greater than six. Table 5 presents the classification accuracy varying the number of hidden layer nodes from 7 to 13.

From Table 5, it is evident that the highest accuracy is achieved with 12 hidden layers. Consequently, 12 hidden layer nodes were selected for the ANN model. A total of 360 samples (90 samples each from the four classes of bearings) were provided as input. The scatter plots of the input data are shown in Figures 7-9.

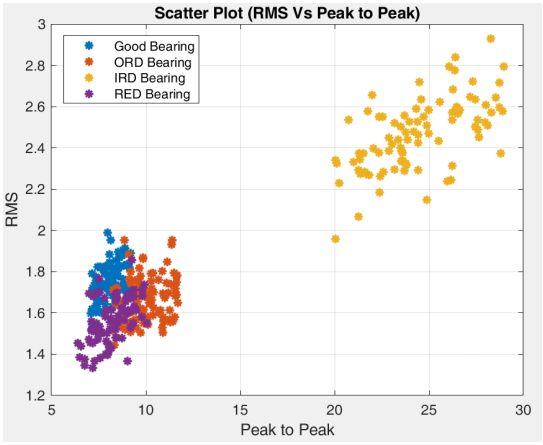

Figure 7. Scatter Plot (RMS Vs Peak)

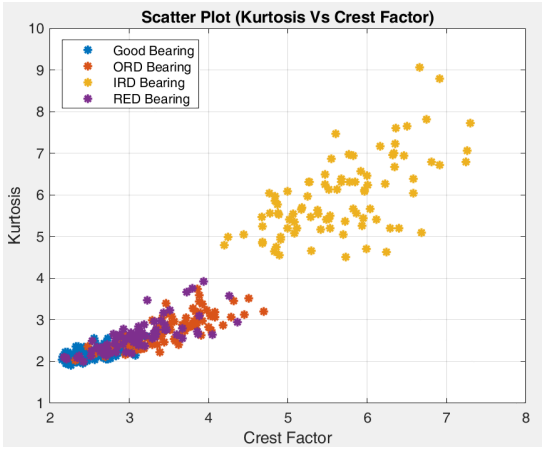

Figure 8. Scatter Plot (Kurtosis Vs Crest Factor)

Table 4. Time Domain Features of Test Bearings

Bearing Condition	Statistical Parameters	RMS	Kurtosis	Crest Factor	Impulse Factor	Peak to Peak	Energy
Good Bearing	Minimum Value	1.54	1.90	2.15	2.53	7.10	11.18
	Maximum Value	1.99	2.66	3.22	3.97	9.23	13.86
	Mean	1.76	2.20	2.55	3.04	8.06	12.65
	Standard Deviation	0.09	0.17	0.28	0.35	0.58	0.60
Bearing with Outer Race Defect	Minimum Value	1.45	2.03	2.32	2.72	8.21	10.12
	Maximum Value	1.95	3.75	4.69	5.74	11.68	14.72
	Mean	1.67	2.74	3.45	4.20	10.04	11.67
	Standard Deviation	0.11	0.37	0.49	0.64	0.99	0.97
Bearing with Inner Race Defect	Minimum Value	1.96	4.51	4.20	5.57	20.05	12.88
	Maximum Value	2.93	9.06	7.30	9.83	28.95	17.19
	Mean	2.46	5.94	5.65	7.48	24.49	15.28
	Standard Deviation	0.17	0.94	0.72	0.98	2.46	0.95
Bearing with Ball Defect	Minimum Value	1.33	2.00	2.17	2.58	6.39	9.25
	Maximum Value	1.86	3.93	4.37	5.23	10.04	12.85
	Mean	1.55	2.58	3.08	3.73	8.14	10.92
	Standard Deviation	0.11	0.38	0.47	0.62	0.94	0.86

Table 5.Classification Accuracy for Different Hidden Layer Nodes

No. of Hidden Layers	7	8	9	10	11	12	13
Accuracy (%)	47	60	63	65	68	87	80

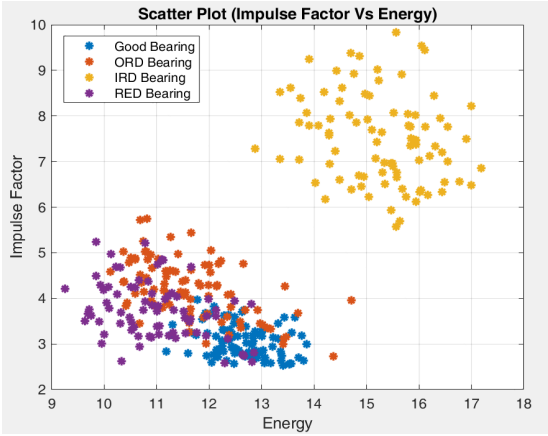

Figure 9. Scatter Plot (Impulse Factor Vs Energy)

This can be observed from the scatter plots as shown in Figures 7-9 that the data points are clustered for good bearings and bearings with defects in the outer race and in rolling element. However, the data points for inner race defects are distinct from the other three classes of bearings.

These samples are categorized into three types: trai–ning samples, validation samples, and testing samples. During training, the network is exposed to training sam–ples and adjusted based on its error. Validation samples are utilized to evaluate the network's generalization ability and to cease training when generalization ceases to improve. Testing samples remain unaffected by training and thus offer an independent assessment of network performance both during and after training. The ANN model randomly allocated 70% of samples for training and reserved 15% for both testing and vali–dation each for LMBP and SCGBP algorithms. How–ever, in the BRBP algorithm, for training 85% samples have been utilized, and the remaining 15% samples have beenused for testing. The ANN model underwent training with these three algorithms, and the respective confusion matrices are displayed in Figures10-12. The cross-entropy (CE) and the mean squared error (MSE) values are presented in Table 6 to compare the per–formance of these three algorithms. Cross-entropy measures the performance of a network by comparing the targets and outputs, with the option to include performance weights and other parameters. A lower cross-entropy value indicates better classifier performance. For each output-target pair, cross-entropy is calculated as (11),

$$CE = -t \times \log(y) \tag{11}$$

where ‘t’ is the target value and ‘y’ is the output value. The overall cross-entropy performance is the average of these individual values. MSE is the average of the squared differences between the outputs and the targets. Lower MSE values indicate better performance, with a value of zero signifying no error.For the arrays of output-target pair, MSE is calculated as (12),

$$MSE = \frac{1}{N}\sum_{i=1}^{N}(y_i - t_i)^2 \tag{12}$$

where 'N' is the number of data points, ‘y_i' is the output value, and 't' is the target value.

In the confusion matrices, the rows represent predicted output values, while the columns display actual target values. In each confusion matrix, correct classifications are represented by green background squares along the diagonal, while misclassifications are indicated by red background squares off the diagonal.

The last row of each matrix displays the percentages of correctly classified samples in green text and misclassified samples in red text, out of the actual samples of a particular class. The square in the last row and last column of each matrix uses a gray background: the percentage of all the correctly classified samples are in green text, and the percentage of all misclassified samples are in red text.

As observed in Figures 10-11,252 samples (70%) were utilized for training, and 54 samples (15%) were utilized for validation and testing each, for the networks trained with LMBP and SCGBP algorithms. However, for the network, trained with BRBP algorithm, 306 samples (85%) and 54 samples (15%) were used for training and testing, respectively. In this algorithm, the generalization took place within the training process without validation. This can be observed fromFigure 12’s validation confusion matrix that all values are zeros. It is evident from Figure 10's all-confusion matrix that each row gives the predicted output values. Out of 90 samples of class 1, 86 were classified correctly, however, 4 were misclassified as fourth class.In the second column, out of 90 samples belonging to class 2, 5 samples were misclassified as class 1 (first row), 75 samples were correctly classified (diagonal element), no sample was misclassified as class 3 (third row), however fourth row shows 10 samples were misclassified as class 4. From the third column, it is evident that al OF THE 90 samples of class 3 wwre classified correctly. And out of 90 samples of class 4, 73 samples were classified correctly, whereas 17 samples were misclassified.

Overall, 90% of the samples were correctly iden–tified and 10% of the samples were misclassified when the network was trained with the lmbp algorithm. Simi–larly, the network, when trained with SCGBP algorithm, gives 83.6% correct classification and 16.4% miscla–ssifications. However, the BRBP algorithm improves the capability of the network in correctly classifying 97.2% samples.The same conclusion can be observedin Table 6; the BRBP algorithm exhibits the highest per–formance in terms of CE and MSE, followed by the LMBP and SCGBP algorithms. Unlike the other three classes, the class 3 samples were 100% correctly classi–fied, without confusion, by all three algorithms. This result is due to the fact that the class 3 data points are distinct from the other three classes of bearings, as seen in the scatter plots.

3.2 Prediction of Bearing Condition by Simulating the Trained ANN

To further evaluate the capability of the network trained with the three algorithms in bearing fault classification, they have been simulated to predict the bearing conditions using a separate dataset of the six time-domain features. The trained ANN models were fed these data for each bearing and the respective predicted values were noted. Table 7 presents a comparison of the predicted values by the three algorithms for the four classes of bearings.

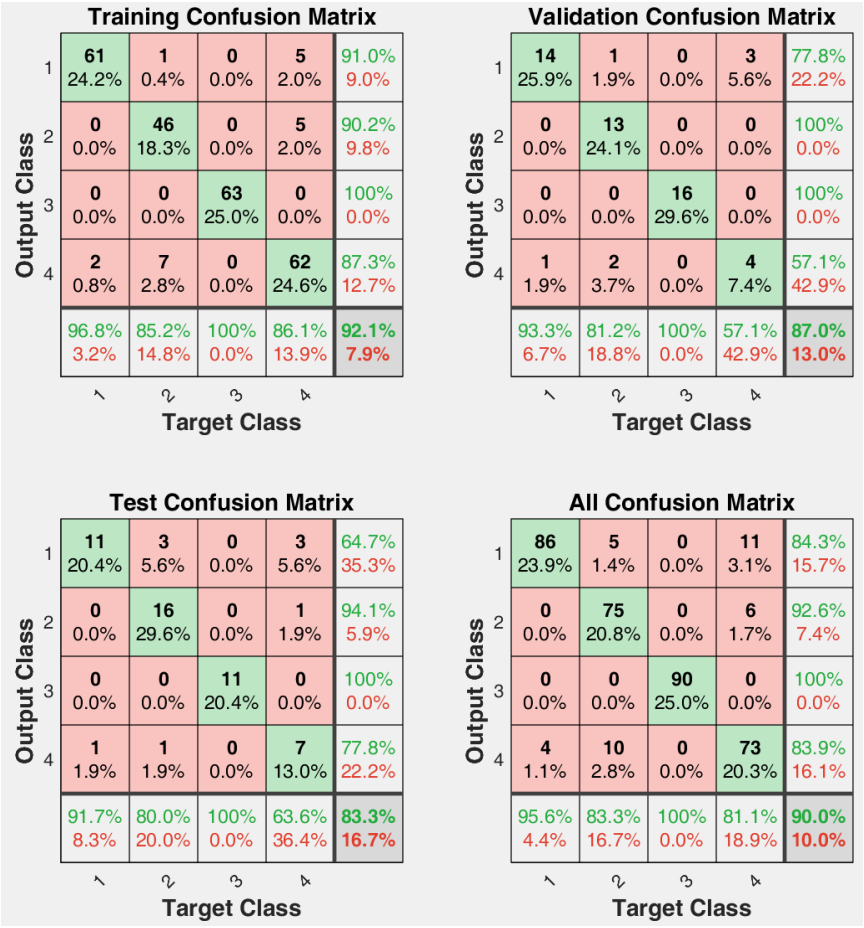

Figure 10. Confusion Matrices for the ANN trained with LMBP Algorithm

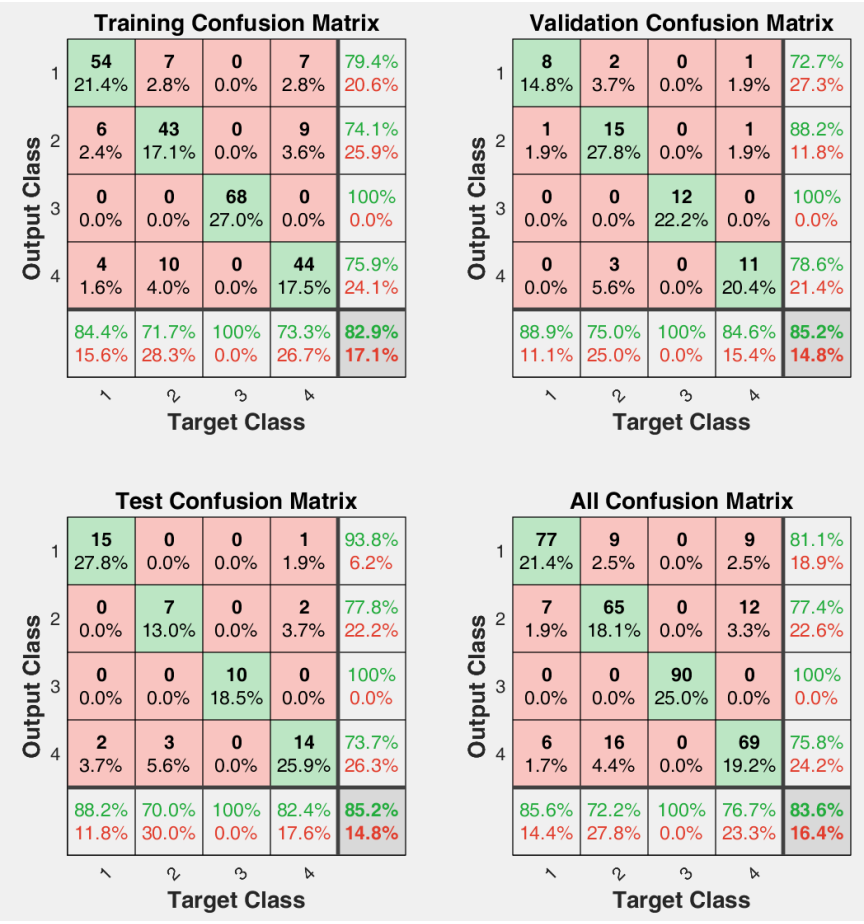

Figure 11. Confusion Matrices for the ANN trained with SCGBP Algorithm

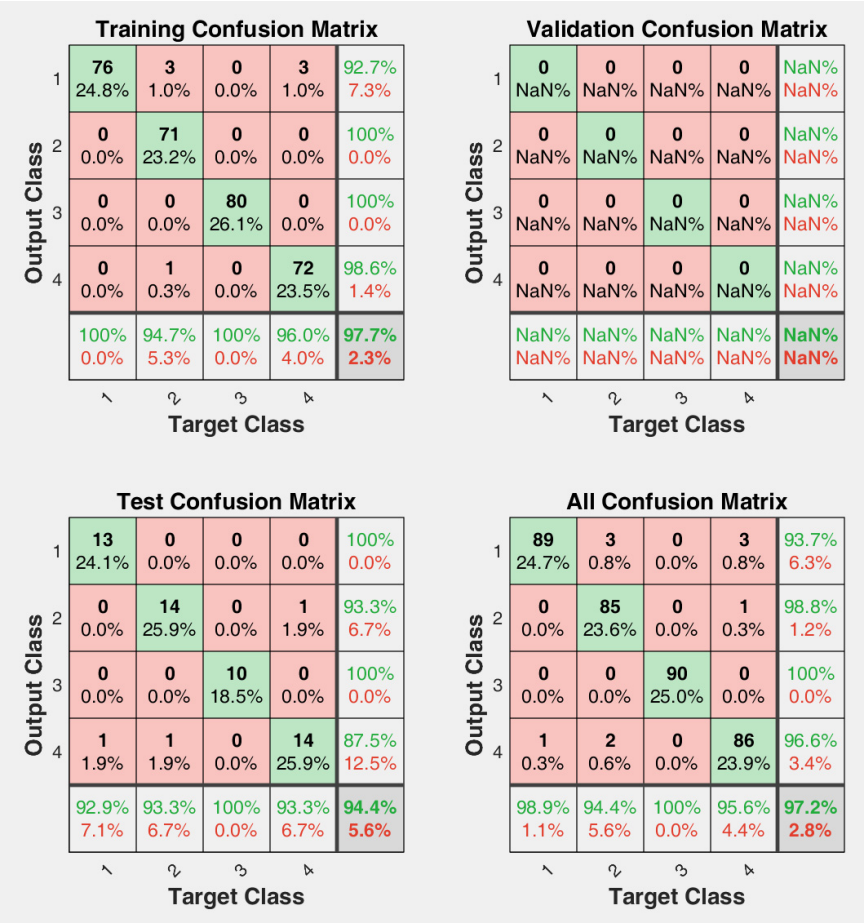

Fig. 12. Confusion Matrices for the ANN trained with BRBP Algorithm

Table 6. Comparison of 3 Algorithms' Performance

Performance Indicator / Algorithm	Cross Entropy (CE)			Mean Squared Error (MSE)		
	Training	Validation	Testing	Training	Validation	Testing
LMBP	0.0500	0.0427	0.0246	0.0511	0.0372	0.0496
SCGBP	1.3682	3.6727	3.7072	0.0529	0.0637	0.0493
BRBP	0.0189	0.0000	0.0408	0.0269	0.0000	0.0565

Table 7. Comparison of Predicted Values with the Target Values for 3 Algorithms in Bearing Fault Classification

BearingCondition	Algorithm / Values	LMBP				SCGBP				BRBP			
Good	Target	1	0	0	0	1	0	0	0	1	0	0	0
	Predicted	0.9891	0.0052	0.0001	0.0056	0.9424	0.0337	0.0002	0.0237	1.0000	0.0000	0.0000	0.0000
	Error	0.0109	0.0052	0.0001	0.0056	0.0576	0.0337	0.0002	0.0237	0.0000	0.0000	0.0000	0.0000
OuterRaceDefect	Target	0	1	0	0	0	1	0	0	0	1	0	0
	Predicted	0.0085	0.9722	0.0040	0.0154	0.0028	0.9957	0.0012	0.0004	0.0000	1.0000	0.0000	0.0000
	Error	0.0085	0.0278	0.0040	0.0154	0.0028	0.0043	0.0012	0.0004	0.0000	0.0000	0.0000	0.0000
InnerRaceDefect	Target	0	0	1	0	0	0	1	0	0	0	1	0
	Predicted	0.0000	0.0006	0.9994	0.0000	0.0000	0.0025	0.9975	0.0000	0.0000	0.0000	1.0000	0.0000
	Error	0.0000	0.0006	0.0006	0.0000	0.0000	0.0025	0.0025	0.0000	0.0000	0.0000	0.0000	0.0000
Ball Defect	Target	0	0	0	1	0	0	0	1	0	0	0	1
	Predicted	0.0000	0.0288	0.0000	0.9711	0.0046	0.0143	0.0000	0.9811	0.0000	0.0000	0.0000	1.0000
	Error	0.0000	0.0288	0.0000	0.0289	0.0046	0.0143	0.0000	0.0189	0.0000	0.0000	0.0000	0.0000

As observed from Table 7, the network with the BRBP algorithm predicts all four classes of bearings with zero errors. The LMBP algorithm performs with higher accuracy than the SCG BP algorithm. Even the networks trained with LMBP and SCG BP algorithms predictminimal errors for inner race defect bearings (class 3).

4. CONCLUSION

Timely fault detection in rotating machinery is crucial to minimize the costs associated with downtime, unexpected failures, and potential casualties. This paper aims at fault diagnosis of rolling element bearings using artificial intelligence techniques,

specifically artificial neural networks. The following conclusions can be drawn:

(1) Experiments were conducted and vibration signals were acquired for the test bearings using NI DAQ and LABVIEW. Six time-domain features were extracted using MATLAB to create a comprehensive dataset for training, validation, and testing of the ANN models.

(2) The networks were trained with three algorithms: Levenberg-Marquardt backpropagation, scaled conjugate gradient backpropagation, and Bayesian regularization backpropagation. It was observed that the BRBP algorithm achieved the highest percentage of correct classification (97.2%), followed by LMBP (90%) and SCGBP (83.6%).

(3) To evaluate their efficacy in bearing fault classi–fication, these three networks were simulated for pre–diction. It was observed that BRBP could predict all four classes of bearings with zero errors from the target values.

The proposed model's accuracy in predicting bea–ring conditions enhances maintenance strategies, pre–venting failures, and extending machinery lifespan. This investigation advances condition monitoring and predictive maintenance, laying the groundwork for future fault diagnosis in mechanical systems.

REFERENCES

[1] D. Abboud, M. Elbadaoui, W. A. Smith, and R. B. Randall, Advanced bearing diagnostics: A compa–rative study of two powerful approaches, Mecha–nical Systems and Signal Processing, Vol. 114, pp. 604–627, 2019, https://doi.org/10.1016/j.ymssp. 2018.05.011

[2] Althubaiti, Adnan, Faris Elasha, Joao Amaral Teixeira. Fault diagnosis and health management of bearings in rotating equipment based on vibration analysis–a review, Journal of Vibroengineering, Vol. 24, no. 1, pp. 46-74, 2022, https://doi.org/10. 21595/jve.2021.22100

[3] P.Y. Kim, I.R.G. Lowe, A review of rolling element bearing health monitoring, In: Proceedings of Machinery Vibration Monitoring and Analysis Meeting, Vibration Institute, Houston, TX, 19–21 April 1983, pp.145–54,

[4] P.D. McFadden, J.D. Smith, Vibration monitoring of rolling element bearings by the high-frequency resonance technique- a review, Tribology Interna–tional, Vol. 17, No. 1, pp. 3-10, 1984.

[5] N. Tandon, B.C. Nakra, Vibration and acoustic monitoring techniques for the detection of defects in rolling element bearings - a review The Shock and Vibration Digest, Vol. 24, No. 3, pp. 3-11, 1992.

[6] N. Tandon, A. Choudhury, A Review of Vibration and Acoustic Measurement Methods for the Detection of Defects in Rolling Element Bearings, Tribology International, Vol. 32, pp.469–480, 1999.

[7] P. Gupta, M. K. Pradhan, Fault detection analysis in rolling element bearing: A review, Materials Today: Proceedings, Vol. 4, No. 2, pp. 2085–2094, 2017, https://doi.org/10.1016/ j.matpr.2017.02.054

[8] I. Howard, A Review of Rolling Element Bearing Vibration "Detection, Diagnosis and Prognosis", Department of Defence, Melbourne, 1994.

[9] A. Rai, S. H. Upadhyay, A review on signal processing techniques utilized in the fault diagnosis of rolling element bearings, Tribology Interna–tional, Vol. 96, pp. 289–306, Apr. 2016, https://doi. org/10.1016/j.trib oint.2015.12.037

[10] M. N. Jagdale, G. Diwakar, A critical review of condition monitoring parameters for fault diagnosis of rolling element bearing, in IOP Conference Se–ries: Materials Science and Engineering, Vol. 455, p. 012090, Dec. 2018, https://doi.org/10.1088/1757-899x/455/ 1/012090

[11] Demetgul, K. Yildiz, S. Taskin, I. N. Tansel, O. Yazicioglu, Fault diagnosis on material handling system using feature selection and data mining techniques, Measurement, Volume 55, pp. 15–24, September 2014, doi.org/10.1016/j.measurement. 2014.04.037

[12] H. Saruhan, S. Sandemir, A. Çiçek, I. Uygur, Vib-ration analysis of rolling element bearings defects, Journal of Applied Research and Technology, Vol. 12, No. 3, pp. 384–395, Jun. 2014, https://doi.org/ 10.1016/s1665-6423(14)71620-7

[13] Q. Xu, S. Lu, W. Jia, C. Jiang, Imbalanced fault diagnosis of rotating machinery via multi-domain feature extraction and cost-sensitive learning, Journal of Intelligent Manufacturing, Vol. 31, No. 6, pp. 1467–1481, 2020, https://doi.org/10.1007/ s10845-019-01522-8

[14] Mohammed, Jawad Saja, Jaber Alaa Abdulhady. Rolling bearing fault detection based on vibration signal analysis and cumulative sum control chart, FME Transactions, Vol. 49, No. 3, pp. 684-695, (2021), doi:10.5937/fme2103684M.

[15] R. Pidl, P. Böröcz, Discrete Fourier transform and cepstrum analysis of vibration events on semitrailer truck, FME Transactions, vol. 47, pp. 177- 182, 2019, doi: 10.5937/fmet1901177P.

[16] J. R. Stack et al, Fault classification and fault signature production for rolling element bearings in electric machines, IEEE Transactions on Industry Applications, Vol. 40, No. 3, pp. 735–739, May 2004, https://doi.org/10.1109/ tia.2004.827454

[17] Kim, Seokgoo An, Dawn Choi, Joo-Ho, Diagnos–tics 101: A Tutorial for Fault Diagnostics of Rolling Element Bearing Using Envelope Analysis in MATLAB, Applied Sciences, Vol. 10. No. 20, 7302, pp. 1-23, 2020, https://doi.org/10.3390/app 10207302

[18] B. Li, M.-Y. Chow, Y. Tipsuwan, J. C. Hung, Neural-network-based motor rolling bearing fault diagnosis, IEEE Transactions on Industrial Elect–ronics, Vol. 47, No. 5, pp. 1060–1069, 2000, https: //doi.org/10.1109/41. 873214

[19] T. Tung, B.-S. Yang, Machine fault diagnosis and prognosis: the state of the art, International Journal of Fluid Machinery and Systems, Vol. 2, No. 1, pp. 61–71, Mar. 2009, https://doi.org/10.5293/ijfms.2009.2.1.061

[20] B. A. Paya, I. I. Esat, M. N. M. Badi, Artificial neural network-based fault diagnostics of rotating machinery using wavelet transforms as a prepro–cessor, Mechanical Systems and Signal Processing, Vol. 11, No. 5, pp. 751–765, Sep. 1997, https://doi. org/10.1006/mssp.1997.0090

[21] P.K. Kankar, S.C. Sharma, S.P. Harsha, Fault Diagnosis of Ball Bearings using Machine Learning Methods, Expert Systems with Applications, Vol. 38, pp. 1876–1886, 2011, https://doi.org/10. 1016 /j.eswa.2010.07.119

[22] J. P. Patel, S. H. Upadhyay, "Comparison between artificial neural network and support vector method for a fault diagnostics in rolling element bearings," Procedia Engineering, Vol. 144, pp. 390– 397, 2016, https://doi.org/10.1016/j.proeng. 2016.05.148

[23] Jamadar, Imran M., Ajit Kumar Patil, Prasanta Kumar Samal, B. Suresha, An empirical model integrating dimensional analysis and Box-Behnken design for crack detection in rotor fan blades, FME Transactions, Vol. 52, No. 1, pp. 45-56, 2024, doi: 10.5937/fme2401045J

[24] Gunerkar, R.S., Jalan, A.K., Belgamwar, S.U. Fault diagnosis of rolling element bearing based on artifi–cial neural network. J Mech Sci Technol 33, 505–511, 2019, https://doi.org/10.1007/s12206-019-0103-x

[25] Harris T. A, Rolling Bearing Analysis, 4th ed., John Wiley & Sons, New York, 2001.

[26] Bishop, Christopher M., and Nasser M. Nasrabadi. Pattern recognition and machine learning, Vol. 4. No. 4. New York: Springer, 2006.

NOMENCLATURE

B	Race Width
d	Ball Diameter
D	Pitch Diameter
fbd	Ball Defect Frequency
fid	Inner Race Defect Frequency
fod	Outer Race Defect Frequency
f_s	Shaft Frequency
ID	Inner Diameter
IF	Impulse Factor
KU	Kurtosis
l	Number of Hidden Layers
m	Number of Output Nodes
n	Number of Input Nodes
z	Number of Balls
ϕ	Contact Angle

ABBREVIATIONS

AI	Artificial Intelligence
ANN	Artificial Neural Network
BP	Back-Propagation
BPFI	Ball Pass Frequency for the Inner Race
BPFO	Ball Pass Frequency for the Outer race
BRBP	Bayesian regularization backpropagation
BSF	Ball Spin Frequency
CF	Crest Factor
CM	Condition Monitoring
EI	Energy Index
FFBP	Feed-Forward Back-Propagation
FFNN	Feed-Forward Neural Network
FFT	Fast Fourier Transform
FTF	Fundamental Train Frequency
LMBP	Levenberg-Marquardt backpropagation
MFS	Machinery Fault Simulator
OD	Outer Diameter
REB	Rolling Element Bearing
RMS	Root Mean Square
SCGBP	scaled conjugate gradient backpropagation
VFD	Variable Frequency Drive

ДИЈАГНОСТИКА КВАРОВА У ЛЕЖАЈЕВИМА КОТРЉАЈУЋИХ ЕЛЕМЕНАТА ПОБОЉШАНА АИ: СВЕОБУХВАТАН ПРИСТУП АНАЛИЗИ ВИБРАЦИЈА

П.К. Самал, К. Сунил, И.М. Јамадар, Р. Сриниди

Ово истраживање представља свеобухватан приступ за дијагностику кварова лежајева кориш–ћењем вештачке интелигенције (АИ), посебно кроз примену вештачких неуронских мрежа (АНН). Интеграцијом ових мрежа у анализу вибрација, приступ има за циљ да задовољи критичну потребу за брзим откривањем квара. Методологија се састоји од три кључна корака: аквизиција сигнала вибрације, издвајање карактеристика и класифи–кација грешке. Експерименти су спроведени за добијање сигнала вибрација за испитне лежајеве на симулатору грешке машине. Шест карактеристика временског домена екстраховано је коришћењем МАТЛАБ-а, стварајући свеобухватан скуп података за обуку АНН модела са три алгоритма: Левенберг-Маркуардт бацкпропагатион (ЛМБП), скалиран коњуговани градијент бацкпропагатион (СЦГБП) и Баиесиан регуларизатион бацкпропагатион (БРБП). БРБП алгоритам је постигао највећу тачну стопу класификације (97,2%), а следе ЛМБП (90%) и СЦГБП (83,6%). Да би се проценила њихова ефикасност у класификацији кварова лежаја, ове три мреже су симулиране, откривајући да БРБП може предвидети све четири класе лежајева са нула грешака.